Exponential convergence method: Nonyrast states, occupation numbers, and a shell-model description of the superdeformed band in ^{56}Ni

Mihai Horoi,[1] B. Alex Brown,[2,3] and Vladimir Zelevinsky[2,3]
[1]*Physics Department, Central Michigan University, Mount Pleasant, Michigan 48859*
[2]*National Superconducting Cyclotron Laboratory, Michigan State University, East Lansing, Michigan 48824*
[3]*Department of Physics and Astronomy, Michigan State University, East Lansing, Michigan 48824*
(Received 3 October 2002; published 12 March 2003)

We suggested earlier that the energies of low-lying states in large shell-model spaces converge to their exact values exponentially as a function of the dimension in progressive truncation. An algorithm based on this exponential convergence method was proposed and successfully used for describing the ground state energies in the lowest $|\Delta(N-Z)|$ nuclides from ^{42}Ca to ^{56}Ni using the fp-shell model and the FPD6 interaction. We extend this algorithm to describe nonyrast states, especially those that exhibit a large collectivity, such as the superdeformed band in ^{56}Ni. We also show that a similar algorithm can be used to calculate expectation values of observables, such as single-particle occupation probabilities.

DOI: 10.1103/PhysRevC.67.034303 PACS number(s): 21.60.Cs, 21.10.Dr, 21.60.Ka, 27.40.+z

The nuclear shell-model calculations are specified by the choice of the active single-particle space (orbitals and their energies), effective interactions and the computational procedure. Full sd-shell-model calculations were possible already 20 years ago [1], but a similar complete calculation for all nuclei in the fp shell is not yet available, although many partial results were already reported [2–5]. The limitations come mainly from the exponential increase of matrix dimensions in many-body Hilbert space with the number of valence nucleons. In the past decade, several approximate methods were proposed to deal with the dimensionality problem. Among them are the shell-model Monte Carlo (SMMC) [6], quantum Monte Carlo diagonalization (QMCD) [7], the $\delta E-\Delta E$ extrapolation method [8], and the exponential convergence method (ECM) [9,10].

The region of the nuclear chart between Ca and Ni is important for coming radioactive beam experiments and astrophysical applications. The interest in the shell-model calculations for nuclei around ^{40}Ca has increased recently with the discovery of superdeformed bands in ^{56}Ni [11], ^{40}Ca [12], and ^{36}Ar [13]. The shell-model description of ^{36}Ar and ^{40}Ca requires a reliable full or partial sd-pf cross-shell effective interaction. This problem is under current investigation, see, e.g., Refs. [14,15]. Positive parity states in ^{56}Ni can be accurately described within fp-model space, for which fairly well tested interactions are available, such as FPD6 [16], KB3 [17], and GPFX1 [18]. However, the KB3 interaction is reportedly not sufficiently accurate around ^{56}Ni [19]. Therefore, it was modified in Ref. [19] by reducing the matrix elements between the $f_{7/2}$ orbit and all other orbits by 300–500 keV. Recently, the matrix elements in this modified version of the KB3 interaction were modified again by another 100 keV and used to describe the first superdeformed band in ^{56}Ni [11] using a $6p$-$6h$ truncated model space, where the particle p and hole h refer to excitations from the $0f_{7/2}$ orbital to one of the $0f_{5/2}$, $1p_{3/2}$, or $1p_{1/2}$ orbitals. The results put the 0_2^+ band head at the right energy of about 4.5 MeV, but the excitation energies do not follow the rotational intervals as closely as the experimental ones [11].

The FPD6 interaction [16] was designed more than a decade ago with the aid of experimental data for lower fp-shell nuclei, and it was later used towards the middle of the fp shell without modifications. The single-particle energies around ^{56}Ni are reasonably well known [18]; small monopole corrections may be required for an accurate description of absolute energies [10]. Although an accurate description of the superdeformed band in ^{56}Ni may require excitations into the $g_{9/2}$ orbit, it was recently reported that the FPD6 predicts a spherical-superdeformed shape coexistence for a series of nuclei, including ^{56}Ni and ^{52}Cr [20–22]. Calculations based on the constrained Hartree-Fock approximation were carried out with the use of more refined approximations, such as the QMCD [22]. The difficulty here lies in calculating the nonyrast 0_2^+ superdeformed band-head state of ^{56}Ni in a reasonably large model space. With the use of the FPD6 interaction within a $6p$-$6h$ truncated model space of about 25×10^6 m-scheme states, the 0_2^+ state comes by 1.6 MeV higher than the value suggested by the experiment [20]. The QMCD calculations [22], however, show the band-head located approximately at the right energy [22]. This result is instructive, indicating that with a relatively small spherical shell-model basis, such as fp, one can successfully describe the coexistence of spherical and superdeformed structure.

In this paper, we will investigate the applicability of the ECM to nonyrast states. The method [9,10] is based on the observation, justified by the analysis of the statistical properties of generic highly excited states [24] and strength functions of simple configurations, that in the process of orderly adding new partitions of given symmetry (spin J, parity, isospin T, etc.) the energy eigenvalues for yrast-states decrease exponentially with the increasing dimension. The reason for this exponential convergence is a subtle coherent pressure of the small admixtures of very complicated remote high-lying states applied through the high orders of perturbation theory. Because of the variational character of the procedure, the convergence is monotonous. The exponential type of the convergence follows [9] from the estimate of the off-diagonal matrix elements after reduction of the Hamiltonian matrix to the tridiagonal form.

In the opposite extreme case, the states at high level density in the middle of the finite shell-model spectrum feel the pressure in both directions, up and down, and their energies do not change monotonously. It is important to understand if the ECM can be extended to the intermediate case of low-lying *nonyrast* states, in particular, if they can be only weakly mixed with yrast states because of different shape of the corresponding mean field. Especially, we are interested in the ability of the ECM to extrapolate the energies of the very collective nonyrast states, such as those of the superdeformed band in ^{56}Ni. In order to understand the applicability of the ECM to such situations, we studied the lowest two 0^+ states in ^{52}Cr that can be calculated for all possible truncation models (maximum *m*-scheme dimension is 46×10^6).

In the ECM, possible configurations of valence nucleons in a finite single-particle space are ordered according to their centroid energies found with the aid of the methods of statistical spectroscopy [23,25]. In a truncation scheme [26] for the low-lying states, higher configurations can be consecutively added to the many-body model space in order of their centroid values. It was shown in Ref. [9] that, as a function of the dimension of truncated Hilbert space, the energies of the low-lying states converge exponentially to their exact values. According to Refs. [9,10], the initial truncation size should exceed a certain value related to the spreading width of typical basis states found from the Hamiltonian matrix prior to its diagonalization. It was also suggested that the matrix elements of observables can be extracted by a similar procedure.

The exponential convergence algorithm for finding the energies of the yrast-states works as follows [9,10]:

(i) A set of configurations (partitions for a given particle number in a certain orbital space) to be included in the calculation is generated. The number of configurations in a given model space is much lower than the shell-model dimension. For example, the highest *m*-scheme dimension for ^{56}Ni in the full fp shell is 1 087 455 228 (the corresponding $JT=00$ dimension is 2 581 576), while the number of partitions is 475.

(ii) The average centroids (Hamiltonian traces divided by the partial dimension) for these configurations are calculated using the prescription of statistical spectroscopy [23,25].

(iii) The configurations are ordered according to their average centroids. This order is different from the usual p particles—h holes scheme. For example, in the fp shell some $8p-8h$ configurations come lower than many of $4p-4h$ configurations. Table I lists the first 131 configurations for ^{56}Ni in order of their centroids.

(iv) Shell-model matrices are built for the truncated spaces consecutively including into calculations the higher partitions in their ''natural'' order established in (iii).

(v) The energies of the yrast states are calculated using a Lanczos eigenvalue solver. The step (v) is repeated 5–10 times by expanding the space with inclusion of new partitions.

(vi) The graph of energy vs JT dimension is plotted (see, e.g., lower panel of Fig. 1), the beginning of the exponential tail is identified, and a fit with the expression

$$E(n)=C+Be^{-\gamma n} \tag{1}$$

is performed. To predict the energy of an yrast state one should evaluate $E(N)$, where N is the full JT dimension of the original model space. In most cases of interest the contribution of the second term in Eq. (1) is small for large values of N, and the value of parameter C represents a good approximation for $E(N)$.

Within the *m*-scheme approach one can easily use the Lanczos algorithm to calculate the lowest states of a given spin and isospin by adding to the nuclear Hamiltonian H_N two terms proportional to the total spin operator squared and total isospin operator squared, which will push up in energy all undesired states of higher spin and isospin,

$$H'=H_N+\alpha\hat{J}^2+\beta\hat{T}^2, \tag{2}$$

where α and β are two parameters conveniently chosen. The set of states with $M=J$ and $T_z=T$ has to be used as an *m*-scheme basis (this choice may forbid taking advantage of the time reversal symmetry in some cases). After the diagonalization, the eigenvalues E' must be rescaled to obtain the true eigenvalues,

$$E=E'-\alpha J(J+1)-\beta T(T+1). \tag{3}$$

The calculations reported below were carried out using the *m*-scheme shell-model code CMICHSM [27].

Figure 1 shows the results for ^{52}Cr using truncated spaces of different JT dimensions. The 315 possible configurations were ordered as described above, and they were progressively included in the shell-model calculations as explained. The upper panel presents the exponential behavior of the energies of 0_1^+ and 0_2^+ states as a function of JT dimension ($JT=00$ for this case as well as for ^{56}Ni). The Coulomb interaction was not included; therefore, isospin T is a good quantum number. The starting dimension in the upper panel is 50 000, about 10% of the full JT dimension (508 289). The lower panel presents in a logarithmic scale the approach to the exponential behavior of the energy value for the 0_2^+ state. For JT dimensions lower than $\approx$50 000, we see a deviation from the exponential behavior. In Ref. [10], we showed that for yrast states the exponential behavior starts approximately at $(3-4)\sigma$ above the configuration with the lowest centroid. Here, σ is the average width of simple shell-model configurations [26,23] found as an average over the partition sum of the off-diagonal matrix elements squared, $\sigma^2=\langle H^2_{\text{off-diag}}\rangle_{\text{av}}$. For nonyrast states, such as the 0_2^+ state in ^{52}Cr, the ''3σ'' rule does not work (the onset of the exponential regime for energy of the 0_1^+ state in ^{52}Cr is still accurately described by this rule). This particular example suggests that using truncated spaces covering 10–12 % of the full JT dimension could be sufficient for predicting the energy of the 0_2^+ state.

Given the similarity between 0_2^+ states in ^{56}Ni and ^{52}Cr [21], we calculated the energy of the 0_2^+ states in ^{56}Ni in truncated spaces of JT dimension up to 12% of the full JT dimension (2.5×10^6) using the collection of configuration listed in Table I. To our knowledge, this is one of the largest

TABLE I. The first 131 single-particle configurations for ^{56}Ni listed in the order of their French and Ratcliff centroids [23] (last column). First four columns indicate the number of particles in each orbit, *m*-dim is the cumulative *m*-scheme dimension and *JT*-dim is the cumulative *JT* dimension.

$n_{f_{7/2}}$	$n_{p_{3/2}}$	$n_{f_{5/2}}$	$n_{p_{1/2}}$	*m*-dim	*JT*-dim	Centroid
16	0	0	0	1	1	−197.566
15	0	1	0	13	1	−190.250
15	1	0	0	21	1	−190.055
15	0	0	1	25	1	−187.505
14	2	0	0	173	5	−183.229
14	0	2	0	479	11	−182.957
14	1	1	0	923	15	−182.854
14	1	0	1	1087	17	−180.567
14	0	1	1	1315	19	−180.289
14	0	0	2	1353	21	−178.340
13	3	0	0	2393	29	−177.088
13	2	1	0	7945	62	−176.143
13	0	3	0	11493	83	−175.686
13	1	2	0	19821	129	−175.676
13	2	0	1	21797	142	−174.314
13	1	1	1	28053	179	−173.466
13	0	2	1	32309	203	−173.095
13	1	0	2	33209	209	−171.975
12	4	0	0	36853	237	−171.631
13	0	1	2	38149	246	−171.222
12	3	1	0	68801	383	−170.117
13	0	0	3	68889	384	−170.069
12	2	2	0	147871	728	−169.080
12	3	0	1	158687	782	−168.746
12	1	3	0	232823	1069	−168.520
12	0	4	0	254579	1177	−168.437
12	2	1	1	313595	1426	−167.328
11	5	0	0	320051	1457	−166.860
12	1	2	1	409279	1809	−166.387
12	2	0	2	417589	1862	−166.294
12	0	3	1	455337	2015	−165.923
12	1	1	2	481845	2136	−164.972
11	4	1	0	565545	2452	−164.776
12	1	0	3	567285	2462	−164.276
12	0	2	2	585381	2557	−164.127
11	4	0	1	614733	2677	−163.862
11	3	2	0	953565	3791	−163.169
12	0	1	3	956073	3805	−163.051
10	6	0	0	961885	3842	−162.773
12	0	0	4	961957	3845	−162.692
11	2	3	0	1506989	5525	−162.039
11	3	1	1	1759553	6394	−161.874
11	1	4	0	2112693	7492	−161.387
11	3	0	2	2147721	7636	−161.298
11	0	5	0	2222537	7890	−161.211
11	2	2	1	2878725	9937	−160.364
10	5	1	0	2996397	10347	−160.119
10	5	0	1	3037545	10503	−159.663
11	2	1	2	3230345	11189	−159.407
9	7	0	0	3232801	11200	−159.371
11	1	3	1	3849725	13073	−159.330
11	2	0	3	3862093	13128	−159.169
11	0	4	1	4041489	13700	−158.774
11	1	2	2	4334021	14679	−157.992
10	4	2	0	5064943	16900	−157.943
11	1	0	4	5065987	16906	−157.473
11	1	1	3	5105731	17066	−157.373
10	4	1	1	5649579	18736	−157.106
11	0	3	2	5773219	19157	−157.055
10	4	0	2	5848161	19453	−156.988
8	8	0	0	5848551	19459	−156.654
10	3	3	0	7694191	24401	−156.243
9	6	0	1	7723687	24513	−156.149
9	6	1	0	7808127	24807	−156.148
11	0	2	3	7835271	24914	−156.055
11	0	1	4	7836783	24922	−155.773
10	3	2	1	10058939	30932	−155.025
10	2	4	0	12106871	36377	−155.021
10	3	0	3	12148019	36533	−154.746
10	3	1	2	12796983	38516	−154.526
10	1	5	0	13757283	41117	−154.275
10	0	6	0	13907961	41620	−154.007
10	2	3	1	17494357	50775	−153.422
9	5	2	0	18314725	53105	−153.401
9	5	0	2	18398569	53397	−153.361
8	7	0	1	18408565	53437	−153.320
9	5	1	1	19018453	55240	−153.022
10	2	0	4	19024265	55277	−152.938
8	7	1	0	19052865	55385	−152.861
10	2	2	2	20744777	60186	−152.542
10	2	1	3	20972133	60937	−152.380
10	1	4	1	23292169	66895	−152.296
10	0	5	1	23779425	68248	−151.647
7	8	0	1	23780677	68255	−151.175
9	4	3	0	26957333	76201	−151.132
10	1	3	2	28549301	80526	−151.035
9	4	0	3	28619569	80770	−151.007
10	1	1	4	28638185	80846	−150.669
10	1	2	3	28983773	81921	−150.492
8	6	0	2	29032155	82116	−150.420
9	4	2	1	32856147	91781	−150.372
9	4	1	2	33969999	94948	−150.330
7	8	1	0	33973571	94964	−150.258
10	0	4	2	34435707	96338	−150.005
8	6	1	1	34786631	97413	−149.623
8	6	2	0	35258927	98861	−149.544
9	3	4	0	40791279	111916	−149.339
9	3	0	4	40806627	111979	−149.087
10	0	3	3	40952703	112444	−149.081
10	0	2	4	40965481	112510	−148.877
9	3	3	1	50666209	134961	−148.198
7	7	0	2	50679445	135015	−148.163
9	3	1	3	51289333	136818	−148.072

TABLE I. (*Continued*).

$n_{f_{7/2}}$	$n_{p_{3/2}}$	$n_{f_{5/2}}$	$n_{p_{1/2}}$	m-dim	JT-dim	Centroid
9	2	5	0	55732425	147346	−148.024
8	5	0	3	55795721	147566	−147.954
9	3	2	2	60359805	159044	−147.776
9	1	6	0	61903957	162959	−147.186
7	7	1	1	61999297	163285	−146.909
9	0	7	0	62180225	163817	−146.826
8	5	1	2	63183389	166667	−146.819
8	5	3	0	66045269	173828	−146.705
6	8	0	2	66046613	173840	−146.592
9	2	4	1	76817145	198134	−146.502
8	5	2	1	80261253	206833	−146.403
7	7	2	0	80389565	207255	−146.372
9	2	1	4	80474005	207549	−146.249
8	4	0	4	80495089	207647	−145.922
9	2	3	2	87869893	225177	−145.699
9	2	2	3	89461465	229477	−145.614
7	6	0	3	89490961	229589	−145.585
9	1	5	1	94526981	241359	−145.284
6	8	1	1	94536457	241399	−144.879
9	0	6	1	95319517	243436	−144.542
8	4	1	3	96160169	245837	−144.449
8	4	4	0	103802577	263501	−144.343
9	1	4	2	108572209	274914	−144.099
7	6	1	2	109037053	276332	−143.993
6	7	0	3	109043577	276360	−143.901
9	1	2	4	109171889	276782	−143.887
6	8	2	0	109184667	276848	−143.885
8	4	2	2	115486605	292335	−143.695

reported model spaces used for a nonyrast state, although a larger one was recently presented in Ref. [5]. Our results are shown in Fig. 2, where the parameters C, B, and γ of Eq. (1) were fitted to the values -198.754, 2.1, and 2.56×10^{-6}, respectively. Equation (1) predicts energy of -198.751 MeV for the 0_2^+ state in ^{56}Ni. This value is consistent with the recent QMCD result of -198.428 MeV [28,22]. The full shell-model calculation of the 0_1^+ state using the FPD6 interaction gives -203.195 MeV [22] (the ECM result is -203.280 MeV [10]). These numbers put the superdeformed 0_2^+ band head at an excitation energy of 4.4–4.5 MeV, which is consistent with experimental data (in Ref. [11] the 0_2^+ was not observed, but it can be extracted from the energies of 2^+ and 4^+ states in the band assuming a perfect rotor behavior).

In Refs. [9,10], we suggested that other observables, besides energies, could exhibit an exponential behavior. The simplest case is given by the expectation values of one-body operators depending on a single state (single JT dimension), such as the electromagnetic moments. For an operator $\hat{O}$, the expectation value in the stationary state $|\alpha\rangle$ that, as a result of the diagonalization, is represented by a complicated superposition of simple shell-model states $|k\rangle$,

$$|\alpha\rangle=\sum_k C_k^\alpha|k\rangle, \tag{4}$$

the expectation value is given by

$$\langle\alpha|\hat{O}|\alpha\rangle=\sum_{kl} C_k^{\alpha*}C_l^\alpha\langle k|\hat{O}|l\rangle. \tag{5}$$

As a first choice for testing the convergence of the expectation values, we take the occupancies of single-particle mean field orbitals, $\nu_j=\Sigma_m a_{jm}^\dagger a_{jm}$. For such a choice, the matrix elements $\langle k|\nu_j|l\rangle$ over the original basis states are diagonal, $k=l$, and, moreover, they are the same for all states $|k\rangle$ from the same partition. Results for electromagnetic moments will be reported elsewhere. Occupation probabilities do not necessarily decrease with the increase of the truncation dimension, as was the case with energies. For nuclei lighter than ^{56}Ni, it is very likely that the occupancy of the $0f_{7/2}$ orbit will decrease, while those of $0f_{5/2}$, $1p_{3/2}$, and $1p_{1/2}$ will increase. The general behavior is expected to be similar to Eq. (1),

$$\nu_j=C_j'+B_j'e^{-\gamma_j' n}. \tag{6}$$

Here, the signs of B_j' are not fixed. When B_j' is positive we plot in logarithmic scale ν_j-C_j' (see lower panel of Fig. 3), while for negative B_j' we plot C_j'-ν_j (see two upper panels in Fig. 3). Figure 3 shows the results for both 0_1^+ and 0_2^+ states in ^{52}Cr. For the 0_2^+ state the exponential behavior takes place for about 90% of the full JT dimension, while for the 0_1^+ the deviation from the exponential law spans a much smaller range.

We notice that the exponents γ_j' are not only nearly equal for different levels j and different states 0_1^+ and 0_2^+ in the same nucleus, they are also quite close to the exponents in the convergence behavior of energies of the same states. Indeed, a simple perturbative estimate gives a hint that the exponents γ and γ' should be close to each other.

To come to this estimate, let us assume that we have diagonalized a truncated matrix containing a number of shell-model partitions of total dimension n. At this stage we have intermediate eigenstates $|\alpha;n\rangle$ and their energies $E_\alpha^{(n)}$ where $\alpha=1,2,\ldots,n$ labels the states inside the given truncation, while the superscript (n) indicates that energy was calculated for this running dimension. Now we add the next partition of dimension d that contains unperturbed states $|k\rangle$ with energies $E_k^{(0)}$ coupled with the states within the diagonalized space by the matrix elements $V_{k\alpha}$. In the exponential regime, the corrections are small and perturbation theory gives the further shift down to the energy of one of the low-lying states $|\alpha\rangle$;

$$E_\alpha^{(n+d)}\approx E_\alpha^{(n)}-\sum_k^d \frac{|V_{k\alpha}|^2}{E_k^{(0)}-E_\alpha^{(n)}}, \tag{7}$$

here and below the Σ_k^d runs over the states of the last partition. Substituting the finite energy shift by the derivative and assuming the exponential convergence (1), we obtain

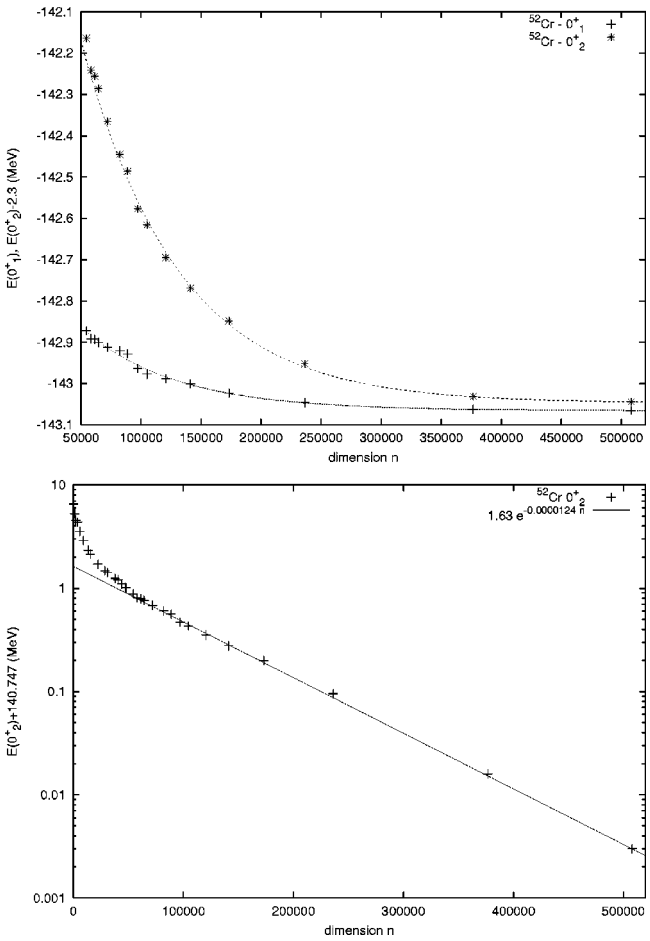

FIG. 1. Energies of the 0_1^+ and 0_2^+ states in ^{52}Cr versus the JT dimension of the truncated space. In the upper panel the energy of the 0_2^+ was artificially shifted down by 2.3 MeV to emphasize its collective character. The lower panel presents only the 0_2^+ state in logarithmic scale to emphasize the exponential behavior.

$$\frac{1}{d}\sum_k^d \frac{|V_{k\alpha}|^2}{E_k^{(0)}-E_\alpha^{(n)}} \simeq \gamma B e^{-\gamma n}. \tag{8}$$

At the same time the correction to the wave function of the state $|\alpha\rangle$ is determined by

$$|\alpha\rangle^{(n+d)} = X|\alpha\rangle^{(n)} + \sum_k^d Y_k|k\rangle, \tag{9}$$

where

$$Y_k = -\frac{V_{k\alpha}}{E_k^{(0)}-E_\alpha^{(n)}} \tag{10}$$

and

$$|X|^2 = 1 - \sum_k^d |Y_k|^2. \tag{11}$$

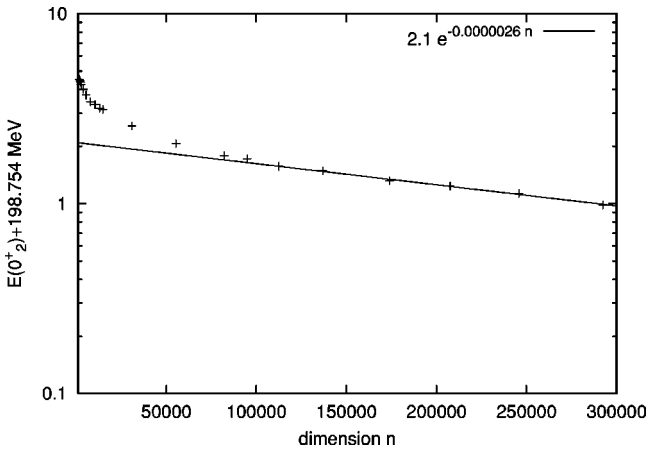

FIG. 2. The exponential convergence of the 0_2^+ state in ^{56}Ni as a function of JT dimension spanning ≈12% of the maximum JT dimension.

In this approximation, we obtain the evolution of the occupation numbers which is, similarly to energy (8), expressed by the second order quantities,

$$\langle\alpha|\nu_j|\alpha\rangle^{(n+d)} = \langle\alpha|\nu_j|\alpha\rangle^{(n)} + \sum_k^d |Y_k|^2[\langle k|\nu_j|k\rangle - \langle\alpha|\nu_j|\alpha\rangle^{(n)}]. \tag{12}$$

It is clear that the population of a given single-particle level grows (decreases) with the admixture of a new partition that has a higher (lower) occupancy of this level. In the derivation of Eq. (12), we took into account that first order matrix elements $\langle\alpha|\nu_j|k\rangle$ vanish because the unperturbed states $|k\rangle$, being orthogonal to the state $|\alpha\rangle$, are the eigenstates of the occupation numbers. By the same reason, the second order admixtures of the states $|l\rangle$ that belong to the new partition also vanish. The only term neglected in Eqs. (9) and (12) is that related to the effective second order mixture (mediated by the states $|k\rangle$ of the last partition) between the states $|\alpha\rangle$ and $|\beta\rangle$ both taken from the previous approximation. This contribution, assuming that $V_{k\alpha}$ are real, is given by

$$\delta(\langle\alpha|\nu_j|\alpha\rangle^{(n)}) = 2\sum_{\beta\neq\alpha}\sum_k^d \frac{V_{\beta k}V_{k\alpha}\langle\alpha|\nu_j|\beta\rangle^{(n)}}{(E_\alpha^{(n)}-E_k^{(0)})(E_\alpha^{(n)}-E_\beta^{(n)})}. \tag{13}$$

In contradistinction to the coherent contributions retained in Eq. (11), this sum contains only incoherent matrix elements between the remote states and no enhancement (well known for the mixing of neutron resonances in the strong parity nonconservation [29]) due to the small energy denominators. Indeed, near a low-lying state $|\alpha\rangle$ the level density is still low, and the spacings $E_\alpha^{(n)}-E_\beta^{(n)}$ are not small.

Since all the states $|k\rangle$ of the last partition have the same occupancies, $\langle k|\nu_j|k\rangle \equiv \overline{\nu_j^{(n)}}$, this stage of the evolution of the occupation numbers is effectively described by

$$\frac{d}{dn}\langle\alpha|\nu_j\alpha\rangle = K_j(n)[\overline{\nu_j^{(n)}} - \langle\alpha|\nu_j|\alpha\rangle], \tag{14}$$

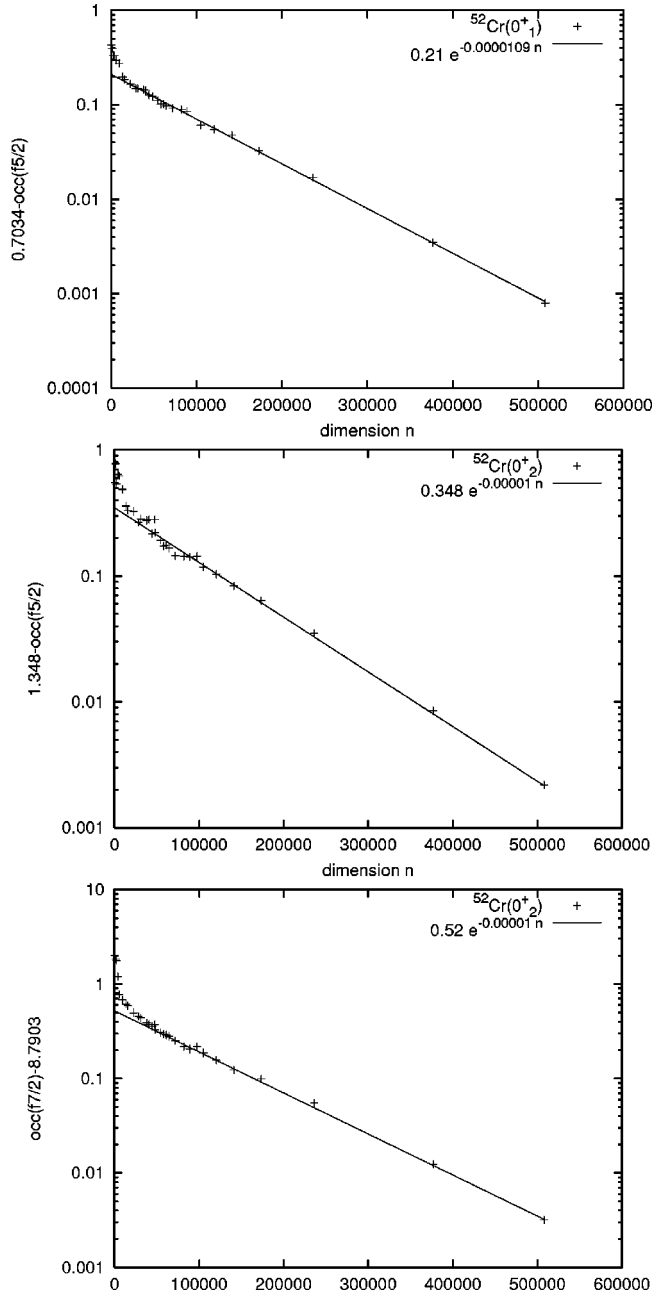

FIG. 3. The exponential convergence of single-particle occupation probabilities ν_j for the 0_1^+ (upper panel, $f_{5/2}$ orbital) and 0_2^+ (two lower panels, $f_{5/2}$ and $f_{7/2}$ orbitals) states in ^{52}Cr as a function of JT dimension.

where

$$K_j(n)=\frac{1}{d}\sum_k^d |Y_k|^2. \tag{15}$$

The main n dependence comes from the factor $K_j(n)$, while the difference $\delta\nu_j$ of occupancies in the square brackets of Eq. (14) is always between 0 and 1 and exponentially fast comes to the limiting value $\overline{\delta\nu_j}$. If the exponential convergence of the occupation numbers takes place, it is determined by

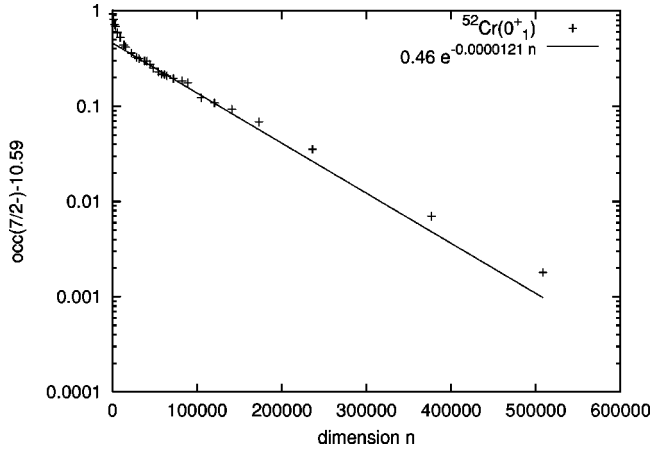

FIG. 4. The exponential convergence of the single-particle occupation probability of the $f_{7/2}$ orbit for the 0_1^+ state in ^{52}Cr described by $\gamma'=0.000121\approx\gamma$.

$$\gamma' B' e^{-\gamma' n}=K_j\overline{\delta\nu_j}. \tag{16}$$

The sum K_j differs from the similar sum in the energy convergence relation (8) by an extra factor $\Delta_{k\alpha}=E_k^{(0)}-E_\alpha^{(n)}$ in the denominator. This factor is only slightly changing within the last partition; therefore, we can expect $\gamma'\approx\gamma$ and $B'\approx B\overline{\delta\nu_j/\Delta}$.

Thus, in a typical case the occupation numbers should converge with the universal exponential rate quite close to that of energies. In the end of the evolution, when the distance from the final value is small, we expect more significant fluctuative deviations. Indeed, we see from Fig. 4 that the fit of the occupancies with $\gamma'=\gamma$ gives a very reasonable agreement up to a region, where $\langle\nu_j\rangle$ differs from the final result by a quantity of the order of 1%. As seen from the derivation, this result is essentially based on the specific properties of the occupation number operator adjusted to the decomposition of the many-body space into partitions.

In conclusion, we have investigated the applicability of the ECM to nonyrast states, in particular, to collective states belonging to superdeformed bands as the ones in ^{56}Ni. Studying similar states in ^{52}Cr, we found that we can apply the ECM to the states of this type by increasing the truncated dimension to $\approx$10% of the full JT dimension. Although this constraint requires more work than in the algorithm for the yrast states [10], it is still much less demanding than the full calculation. Our results indicate that a relatively small spherical single-particle model space, such as fp, and the unmodified FPD6 interaction are able to describe very well the superdeformed band in ^{56}Ni. We also show that occupation probabilities follow exponential behavior similar to that of energies. In a good approximation, their rate of convergence coincides with that of energies due to the specific properties of the occupation number operator and the way of organizing the shell-model partitions. Investigation of other observables, such as the electromagnetic moments, can be of great practical interest.

The authors acknowledge support from the NSF Grant Nos. PHY-0070911 and DMR-9977582.

[1] B.A. Brown and B.H. Wildenthal, Annu. Rev. Nucl. Part. Sci. **38**, 29 (1988).
[2] E. Caurier, G. Martinez-Pinedo, F. Nowacki, A. Poves, J. Retamosa, and A.P. Zucker, Phys. Rev. C **59**, 2033 (1999).
[3] C. Mazzocchi *et al.*, Eur. Phys. J. A **12**, 269 (2001).
[4] E. Caurier, G. Martinez-Pinedo, F. Nowacki, A. Poves, J. Retamosa, and A.P. Zucker, Nucl. Phys. **A654**, 747c (1999).
[5] F. Nowacki, Nucl. Phys. **A704**, 223c (2002).
[6] D.J. Dean, P.B. Radha, K. Langanke, Y. Alhassid, S.E. Koonin, and W.E. Ormand, Phys. Rev. Lett. **72**, 4066 (1994); Y. Alhassid, D.J. Dean, S.E. Koonin, G. Lang, and W.E. Ormand, *ibid.* **72**, 613 (1994).
[7] M. Honma, T. Mizusaki, and T. Otsuka, Phys. Rev. Lett. **75**, 1284 (1995); **77**, 3315 (1996).
[8] T. Mizusaki and M. Imada, Phys. Rev. C **65**, 064319 (2002).
[9] M. Horoi, A. Volya, and V. Zelevinsky, Phys. Rev. Lett. **82**, 2064 (1999).
[10] M. Horoi, B.A. Brown, and V. Zelevinsky, Phys. Rev. C **65**, 027303 (2002).
[11] D. Rudolph *et al.*, Phys. Rev. Lett. **82**, 3763 (1999).
[12] E. Ideguchi *et al.*, Phys. Rev. Lett. **87**, 222501 (2001).
[13] C.E. Svensson *et al.*, Phys. Rev. C **63**, 061301(R) (2001).
[14] E. Caurier, K. Langanke, G. Martinez-Pinedo, F. Nowacki, and P. Vogel, Phys. Lett. B **522**, 240 (2001).
[15] E. Caurier, F. Nowacki, A. Poves, and A. Zuker, nucl-th/0205036.
[16] W.A. Richter, M.G. van der Merwe, R.E. Julies, and B.A. Brown, Nucl. Phys. **A523**, 325 (1991).
[17] A. Poves and A.P. Zuker, Phys. Rep. **70**, 235 (1981).
[18] M. Honma, T. Otsuka, B.A. Brown, and T. Mizusaki, Phys. Rev. C **65**, 061301(R) (2002).
[19] G. Martinez-Pinedo, A.P. Zuker, A. Poves, and E. Caurier, Phys. Rev. C **55**, 187 (1997).
[20] T. Mizusaki, T. Otsuka, Y. Utsuno, M. Honma, and T. Sebe, Phys. Rev. C **59**, R1846 (1999).
[21] T. Mizusaki, T. Otsuka, M. Honma, and B.A. Brown, Phys. Rev. C **63**, 044306 (2001).
[22] T. Otsuka, M. Honma, T. Mizusaki, N. Shimizu, and Y. Utsuno, Prog. Part. Nucl. Phys. **47**, 319 (2001).
[23] J.B. French and K.F. Ratcliff, Phys. Rev. C **3**, 94 (1971).
[24] V. Zelevinsky, B.A. Brown, N. Frazier, and M. Horoi, Phys. Rep. **276**, 85 (1996).
[25] S. S. M. Wong, *Nuclear Statistical Spectroscopy* (Oxford University Press, New York, 1986).
[26] M. Horoi, B.A. Brown, and V. Zelevinsky, Phys. Rev. C **50**, R2274 (1994).
[27] Mihai Horoi, Advanced Computational Methods for Solving the Nuclear Many-Body Problem, Institute for Nuclear Theory, Seattle, WA, 2002, http://mocha.phys.washington.edu/~int_talk/WorkShops/ACD02/
[28] T. Mizusaki (private communication).
[29] V.V. Flambaum and G.F. Gribakin, Prog. Part. Nucl. Phys. **35**, 423 (1995).